Available online at www.CivileJournal.org

Civil Engineering Journal

(E-ISSN: 2476-3055; ISSN: 2676-6957)

Vol. 10, Special Issue, 2024

"Sustainable Infrastructure and Structural Engineering: Innovations in Construction and Design"

Evaluating Axial Strength of Cold-formed C-Section Steel Columns Filled with Green High-performance Concrete

Al Mashhadani D. A. Jasim [1, 2*], Leong Sing Wong [1, 2], Ahmed W. Al-Zand [3], Sih Ying Kong [4]

[1] *Department of Civil Engineering, College of Engineering, Universiti Tenaga Nasional, Jalan IKRAM-UNITEN, 43000 Kajang, Selangor, Malaysia.*

[2] *Institute of Energy Infrastructure, Universiti Tenaga Nasional, Jalan IKRAM-UNITEN, 43000 Kajang, Selangor, Malaysia.*

[3] *Department of Civil Engineering, Universiti Kebangsaan Malaysia (UKM), 43600 Bangi, Selangor, Malaysia.*

[4] *Discipline of Civil Engineering, School of Engineering, Monash University Malaysia, 47500 Bandar Sunway, Selangor, Malaysia.*

Received 29 August 2024; Revised 22 November 2024; Accepted 05 December 2024; Published 16 December 2024

Abstract

Concrete-filled steel tube (CFST) columns that experience outward local buckling under high axial stress remain a significant concern, particularly when thin steel sections are used, as opposed to semi-compact and compact sections. This study investigated the performance of column systems by comparing single- and double-C-section configurations with both hollow and concrete-filled designs. Two types of infill materials were investigated: normal concrete and recycled material concrete, which included 10% waste glass powder as a cement replacement, 8% black high-density polyethylene beads as a sand substitute, and 10% pumice stone as coarse aggregate. To enhance the strength of the proposed CFS column, steel strips and screws were used to connect the flanges of the C-sections. Nine columns were tested experimentally under static axial load. Additionally, finite element analysis software was used to model and evaluate the effects of parameters beyond those investigated in the tests. The results indicated that the load capacity of the double face-to-face section was approximately 3% higher than that of the double back-to-back section. The addition of steel strips, used to connect the lips of the C-section flanges, enhanced the axial strength of the column by approximately 2% compared with the unstrengthened corresponding specimen and delayed buckling in the most vulnerable areas. Furthermore, the recycled infill concrete material had a minimal impact on the axial performance of the analyzed CFS columns compared to the control concrete, with a difference of less than 2.2%. The findings confirm that recycled waste material concrete can achieve performance comparable to that of the conventional concrete.

Keywords: Cold Formed Steel Column; Failure Modes; Confinement; Axial Load; Optimized Concrete.

1. Introduction

The use of cold-formed steel (CFS) in the construction industry is increasing. CFS columns are widely used in racks, portal frames, roof trusses, and residential buildings in the construction industry due to their excellent energy efficiency and resource utilization. However, CFS members are prone to structural instabilities because of their high cross-sectional slenderness and the use of high-strength steel for thickness reduction. Concrete-filled steel tubes (CFST) have

* Corresponding author: pe21300@student.uniten.edu.my

http://dx.doi.org/10.28991/CEJ-SP2024-010-014

demonstrated superior performance in modern construction, showing improved strength, ductility, and stiffness compared to conventional concrete or steel elements under axial and flexural loading [1–4].

The structural behavior of CFST composite elements has been extensively studied through experimental and numerical investigations, covering a range of CFST forms, including circular CFST beams and columns [5], elliptical members [6], rectangular structures [7, 8], square and rectangular steel tubes [9], reinforced concrete (RC) columns under compression and bending loads [10], composite tubes filled with concrete [11-14], and concrete-filled steel profiled wall and slab systems [15, 16]. Other designs, such as built-up stiffened box sections [17, 18], box-shaped built-up columns [19], and sigma and lipped channels [20], have also been investigated.

Innovative and optimized cross-sectional designs have enhanced the structural performance of CFS elements [21, 22]. Nonetheless, thin structural elements remain vulnerable to outward buckling under compressive stress [11, 12]. Internal steel stiffeners have been employed to mitigate buckling in thin cross-sections of CFST beams [13-16]. The application of steel strips to reinforce concrete-filled C-sections has notably enhanced the composite behavior of specimens, improving their buckling capacities. In this experimental study, increased load capacity was achieved using screw connectors or steel strips [23]. Previous studies have investigated the flexural performance of various C-sections with different dimensions, thicknesses, and connection methods, including the stiffening of a single C-section beam connected by a number of steel strips, internal stiffening of a double C-section beam, and the use of CFRP sheets to strengthen a novel C-section beam [24, 25]. These investigations aimed to assess the efficiency of stiffening and performance of lightweight, recycled-material-based concrete in a new steel–concrete composite beam system.

The growing concern over environmental pollution from waste disposal has intensified efforts to restore ecological balance. Recycling waste materials to produce high-performance concrete (HPC) has emerged as a promising sustainable construction practice aimed at long-term environmental well-being. Engineers have promptly begun integrating selected waste materials into concrete mixes and repurposing them as recycled aggregates for construction applications [26-30]. Numerous studies have focused on CFST elements infused with recycled aggregate concrete (RAC) [31, 32]. In recent years, recycled aggregates generated from waste materials have been increasingly used in construction. Extensive research has investigated the performance of concrete containing recycled waste materials, such as waste glass powder [33, 34], recycled plastic high-density polyethylene (HDPE) [35-37], and pumice stone aggregate (PSA) [38, 39].

This study evaluated the compression performance of single and double C-sections connected with outer steel strips filled with high-performance concrete optimized with recycled waste materials. Specifically, waste glass powder replaced cement, black HDPE beads substituted sand, and PSA served as coarse aggregates. The study aimed to evaluate the feasibility of novel cold-formed tubular cross-sections made from two C-section components, connected either double face-to-face (F-F) or double back-to-back (B-B). Furthermore, the research explored the behavior of the proposed CFST columns integrating high-performance concrete with recycled waste materials. The columns were tested based on three groups: hollow, normal concrete-filled, and optimized green concrete-filled, using different configurations of cold-formed tubular cross-sections (single, B-B, and F-F) strengthened by steel strips connected with self-tapping screws. The experimental results included axial load capacity, failure modes, load versus longitudinal displacement, stiffness, and ductility index. The finite element (FE) models were validated against the experimental results and then used for further parametric studies.

2. Experimental Program

2.1. Descriptions of Specimens

Rectangular tube columns were created by connecting CFS C-sections in three configurations: single, double face-to-face, and double back-to-back. The columns were filled with either normal concrete or optimized green concrete containing waste glass powder, HDPE, and PSA. The C-section dimensions were as follows: depth of 150 mm, flange width of 65 mm, lip size of 16 mm, and thickness of 1.6 mm. Figure 1 illustrates the work process methodology employed in this study. The resulting specimens, each measuring 1.5 m in length (Figure 2), were divided into three groups for testing. Group 1 comprised three specimens intended as control models with hollow sections. Group 2 included three specimens to explore the impact of different waste materials (10% WGP, 8% HDPE black beads, and 10% PSA) on the concrete filling. Group 3 included three specimens filled with normal concrete and subjected to static compression loading. To enhance the strength of the fabricated tubular columns, steel strips were affixed at the top, center, and bottom (as shown in Figure 3) to counteract buckling failure. Table 1 lists the designations and specifications of the CFST specimens used in this study. The specimens were labeled as follows: H for hollow; F for filled concrete; S for single sections; and D for double sections. After casting, the specimens were cured at room temperature for 30 d before testing.

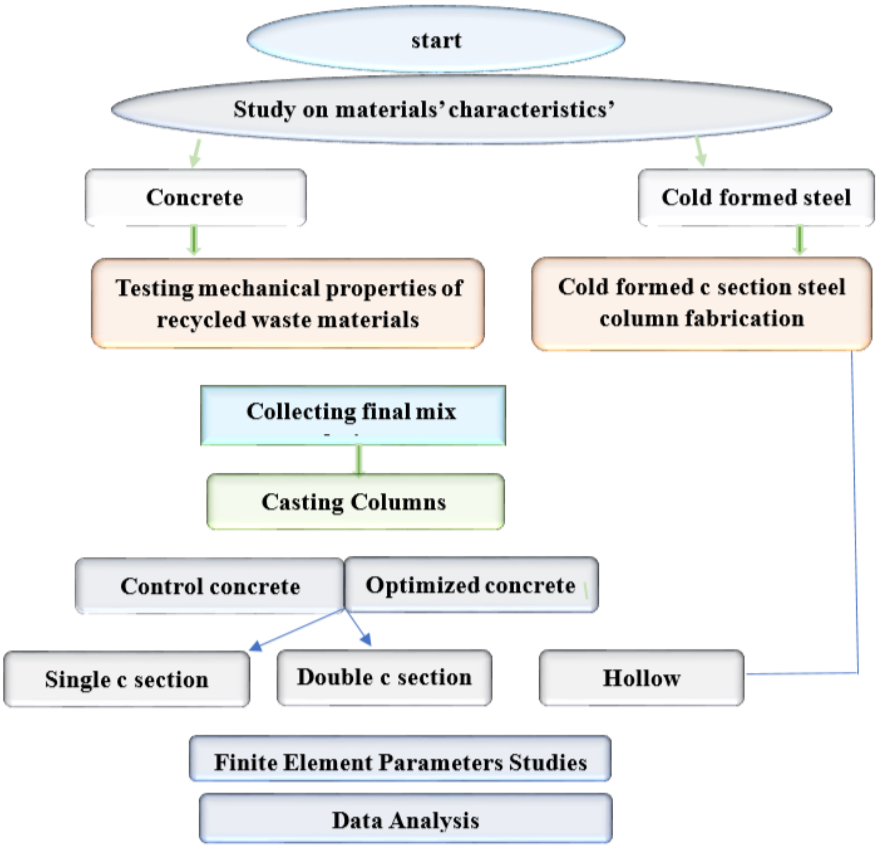

Figure 1. Research Methodology

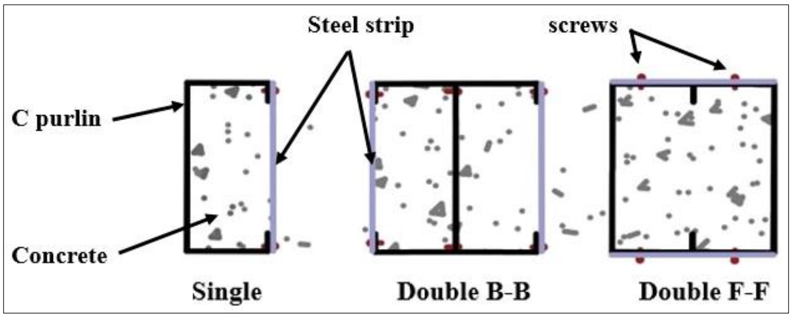

Figure 2. Column section

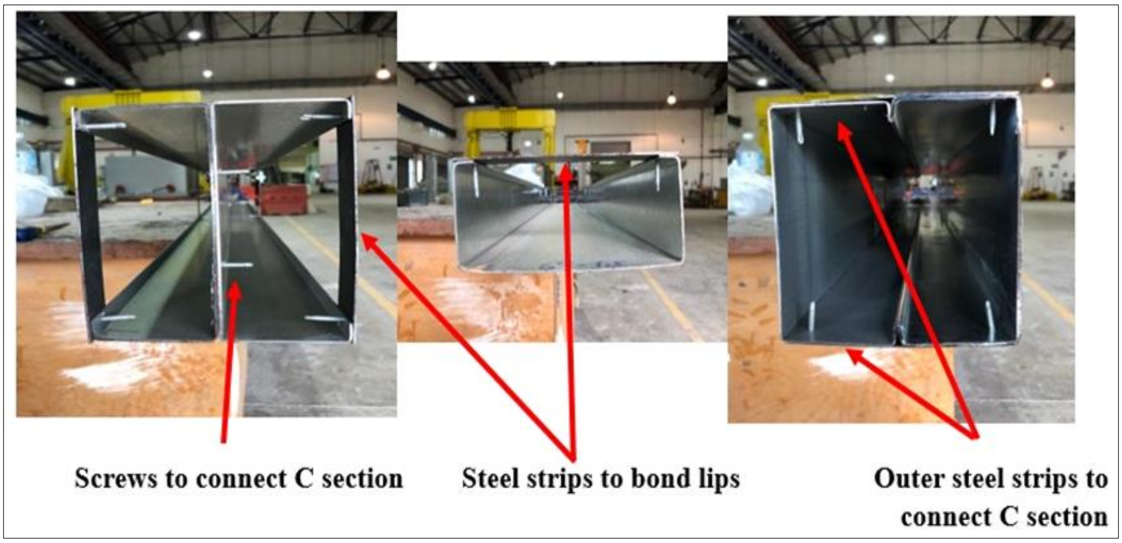

Figure 3. Steel strips and screws to connect the C sections and outer tube

Table 1. Details of the CFST specimens

Group No.	Specimens Designation	D×B×t (mm)	Length Le (m)	Fy (MPa)	Concrete infill type	No of steel strips	Spacing between strips (mm)
Group 1	SH	150×65×1.6	1.5	489	Hollow	3	750
	DB-BH	150×130×1.6	1.5	489	Hollow	6	750
	DF-FH	150×130×1.6	1.5	489	Hollow	6	750
Group 2	SFCC	150×65×1.6	1.5	489	Control Concrete	3	750
	DB-BFCC	150×130×1.6	1.5	489	Control Concrete	6	750
	DF-FFCC	150×130×1.6	1.5	489	Control Concrete	6	750
Group 3	SFOC	150×65×1.6	1.5	489	Optimized concrete	3	750
	DB-BFOC	150×130×1.6	1.5	489	Optimized concrete	6	750
	DF-FFOC	150×130×1.6	1.5	489	Optimized concrete	6	750

2.2. Material Characteristics

The mechanical properties of the C-section steel were thoroughly analyzed. According to the ASTME8/E8M-2009 standard, three test coupons were subjected to direct tensile loading. The average values obtained from the tensile tests revealed an ultimate tensile strength (fu) of 558 MPa, a yield tensile strength (fy) of 489 MPa, maximum elongation of 27.4%, and modulus of elasticity (Es) of 201 GPa.

In the concrete formulations, the base mixture was composed of normal concrete (NC). However, in the modified mixture, 28% of the standard concrete components were replaced with 10% waste glass powder, 8% HDPE beads, and 10% pumice stone. As illustrated in Figure 4, the particle size of the waste glass powder ranges from 100 to 700 microns, with a density of 1455.5 kg/m³. The HDPE beads have diameters between 1.8 and 3.6 mm and a density of 595 kg/m³, while the pumice stone aggregate (PSA) ranges in size from 1 mm to 20 mm with a density of 473 kg/m³. All concrete mixtures maintained a water-to-cement ratio of 0.30, and a superplasticizer was incorporated at 1.5% of the cement weight for specific mixes.

(a) (b) (c)

Figure 4. Concrete materials replacement (a) WGP with cement (b) HDPE with sand (c) PSA with coarse aggregate

2.3. Test Setup

The constructed CFST specimens were statically loaded using a hydraulic jack with a maximum capacity of 1000 kN. The load was applied progressively. The displacement of the specimens at the center was measured using linear variable displacement transducers (LVDTs). Compressive stress on the steel tube surfaces was measured using 30-mm strain gauges. Three strain gauges (SG1–SG3) were positioned at the top, center, and bottom of each specimen. The test configuration is shown in Figure 5. Data from the load cells, LVDTs, and strain gauges were collected using a data logger and recorded on a computer system for each loading stage.

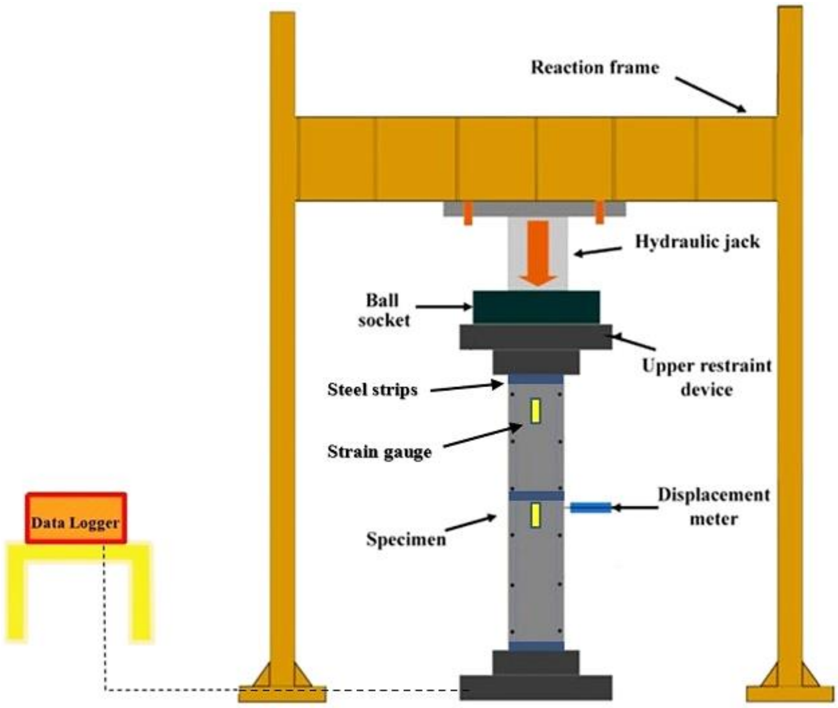

Figure 5. Schematic diagram of axial compression test for CFST specimens

3. Results

3.1. Concrete Compressive Strength

Figure 6 presents findings that demonstrate a similar trend in the performance of compressive strength tests. The cube compressive strength of the control specimen was found to be 51.5 MPa. The compressive strengths of the waste glass concrete mixes at 28 d are presented in Figure 6-a, which illustrates the increment ratios in compressive strength. According to the test results, the highest 28-day compressive strength value of 52.3 MPa was obtained from the concrete mix made of 10% waste glass cement, representing an increase of 1.54% compared to the control mix. Pozzolanic reactions appear to counteract this trend at later stages of hardening, contributing to improved compressive strength at 28 d. A similar observation was reported by Metwally [40], where the author concluded that significant strength enhancement occurred when the pozzolanic effect became pronounced at a late age of 28 d. The compressive strength using waste HDPE beads indicated an increase at both 5% and 8% replacement levels but decreased with higher replacement amounts.

The test results indicated a compressive strength value of 54.1 MPa for the concrete mix with 8% waste HDPE, representing an increase in the compressive strength of 5% compared to the control mix, as shown in Figure 6-b. The reduction in compressive strength may be attributed to the decreased force between the paste and the plastic surface, as well as the hydrophobic nature of the plastic, which can hinder cement hydration [36]. The compressive strength was determined for each sample using a different percentage of PSA replacing coarse aggregate to evaluate the impacts on the strength of high-performance concrete. The compressive strengths of the PSA concrete mixes are presented in Figure 6-c. The strength development up to 28 d showed a highest strength of 51.4 MPa at 10% PSA, which is almost similar to the control mix with a 51.5 MPa compressive strength. However, increasing the amount of PSA above 10% resulted in a reduction in compressive strength. This decrease may be attributed to the greater water absorption of the pumice stone compared to normal coarse aggregate, due to higher porosity [41, 42]. Finally, a combination replacement of 10% WGP as cement, 8% waste HDPE as fine aggregate, and 10% PSA as coarse aggregate for the concrete was evaluated. The results indicated that this combination of waste materials achieved high-performance concrete compared to the reference mix. The optimized concrete contents are presented in Table 2.

Table 2. Mix design proportion

Mix	Gravel: sand: cement	w/c ratio	Superplasticizer %	% WGP replacement of cement	% HDPE replacement of sand	% PSA replacement of gravel	Density (kg/m³)	Compressive Strength fcu (MPa)
Normal	2:1:1	0.3	1.5	0	0	0	2400	51.5
Optimized	2:1:1	0.3	1.5	10%	8%	10%	2325	50.1

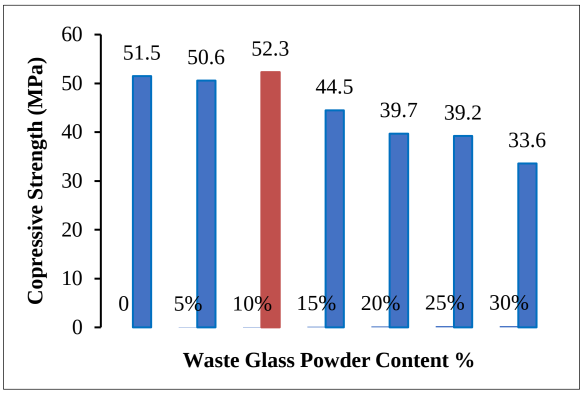

(a)

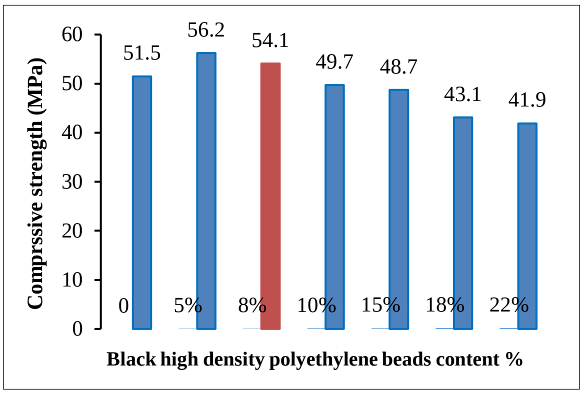

(b)

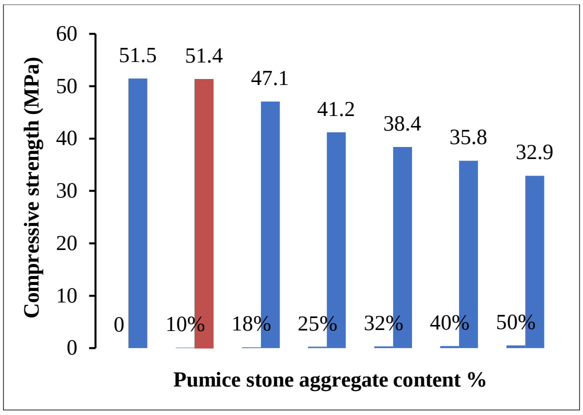

(c)

Figure 6. Compressive strength results of the materials used

3.2. Failure Modes

This section discusses the failure modes observed in experimental trials involving specimens composed of CFS C-sections. These specimens were subjected to testing beyond their ultimate capacities to investigate compression performance failure. The columns were categorized into three groups. The initial group consisted of hollow C-sections, including a single hollow section (SH), double back-to-back hollow section (DB-BH), and double face-to-face hollow section (DF-FH). These sections experienced outward tube buckling failure in the region between the top and center. To mitigate this buckling, steel strips were strategically positioned at the top, center, and bottom. These strips delayed inward buckling failure due to the dual-section configuration. As the load was gradually increased, the tube failure gradually intensified, as shown in Figure 7. Outward buckling was observed in the load-bearing regions at the top and bottom, where the sections were supported with steel strips positioned at these locations. The double sections displayed nearly identical failure patterns with consistent displacements.

(a)

(b)

(c)

Figure 7. Failure mode of the hollow (a) SH (b) DB-BH (c) DF-FH sections

The behavior of single sections filled with both standard control concrete (SFCC) and concrete incorporating recycled materials (SFOC) was examined. Notably, the single section filled with control concrete show buckling in the lower support region, whereas its counterpart filled with recycled material concrete in the upper load-bearing area. Despite this difference, both sections demonstrated similar failure characteristics at the same displacement, as shown in Figure 8.

(a) (b) (c)

Figure 8. Failure mode of the single filled (a) control concrete (b) original sample (c) optimized concrete

The double back-to-back section filled with control concrete (DB-BCC) failed at the supporting zone. Conversely, the double back-to-back section utilizing optimized concrete (DB-BOC) failed at the bottom and center, where it was supported by steel strips, as depicted in Figure 9. In the subsequent phase, the performance of the double sections was assessed when F-F was filled with control concrete and recycled material replacement concrete (DF-FCC) and with optimized concrete (DF-FOC). The flanges of these sections were reinforced with steel strips at the top, center, and bottom. These sections exhibited the same failure pattern, with failure occurring at the support and load-bearing regions, as depicted in Figure 10. However, the section filled with control concrete exhibited a delayed failure, likely due to less concrete confinement in the double back-to-back C-section. This resulted in significant cracking and sliding of the concrete and steel tube at the point of maximum load, which was not observed in the double F-FCC-sections.

(a) (b) (c)

Figure 9. Failure mode of the DB-B section (a) control mix (b) original sample (c) optimized mix

(a) (b) (c)

Figure 10. Failure mode of the DF-F section (a) control mix (b) original sample (c) optimized mix

The failure modes indicate that the steel strips can resist buckling, especially at the center. Improving the effectiveness of these steel strips requires stronger connections at the upper and lower flanges of each individual cold-formed C-section. This stage is essential for enhancing the restraining capability of the concrete core within the newly developed composite column structure. A strong bond was formed between the concrete core by enclosing 16 mm lips around the top and bottom margins of the prefabricated cold-formed C-sections. These lips acted as internal reinforcements for the upper and lower flanges inside the steel tube, as shown in Figure 3. Notably, the results were comparable to those achieved using additional steel stiffeners in previous studies to improve the structural integrity of slender CFST members [43, 44].

Joining the two face-to-face C-sections improves performance under axial loads and creates a thin steel tube column filled with concrete and internal steel stiffeners. Because it is difficult to contain the infill concrete along the open side of the C-section, where the core concrete may leak, a single C-section in a concrete-filled tube composite system exhibits distinct failure modes than two C-sections linked together.

3.3. Load-Displacement Relationship

The experimental test of the axial load-displacement curves demonstrated remarkable consistency across the repetitions of each configuration. Analysis of the axial load versus axial shortening behavior of the tested specimens revealed a linear load-deformation trend up to their respective peak capacities. The ultimate axial resistances of the SHS, DB-BHS, and DF-FHS specimens were 79.14, 167.6, and 164.3 kN, respectively, with axial displacement ranging from 1.5–2 mm, as depicted in Figure 11-a. The single-section test specimens displayed half of the ultimate load compared to the double-section counterparts. When comparing the behavior of the double sections, the back-to-back arrangement displayed slightly higher load and displacement values than the face-to-face sections. This phenomenon is attributed to the double web thickness at the center, reinforced by screws [45], and the outer lips reinforced by steel strips. The SH, SFCC, and SFOC specimens exhibited ultimate axial resistances of 79.14, 442, and 431.9 kN, respectively, with axial displacement between 1.75–2.75 mm, as illustrated in Figure 11-b. Notably, the single-filled column test specimens demonstrated similar ultimate loads and displacements, indicating analogous behavior between the C-section filled with regular concrete and those with partially replaced recycled material concrete. This consistency can be attributed to the similar geometries and concrete strengths of the mixtures. For the DB-BHC, DB-BCC, and DB-BOC specimens, the ultimate axial resistances of 167.6, 858, and 817.6 kN were recorded, with corresponding axial displacements between 2–3 mm, as depicted in Figure 11-c. As expected, the double-backfilled column test specimens exhibited identical ultimate loads. The DF-FH, DF-FCS, and DF-FOS specimens showed ultimate axial resistance values of 164.3, 886.4, and 870.8 kN, respectively, with axial displacements ranging from 1.5–3 mm. As shown in Figure 11-d, the double-faced, face-filled column test specimens exhibited nearly identical ultimate loads, with an 81% higher load capacity than the hollow section. The results indicate that the double f-f section outperformed the b-b section, as the full confinement and the presence of lips enhanced buckling resistance, thereby improving loading capacity.

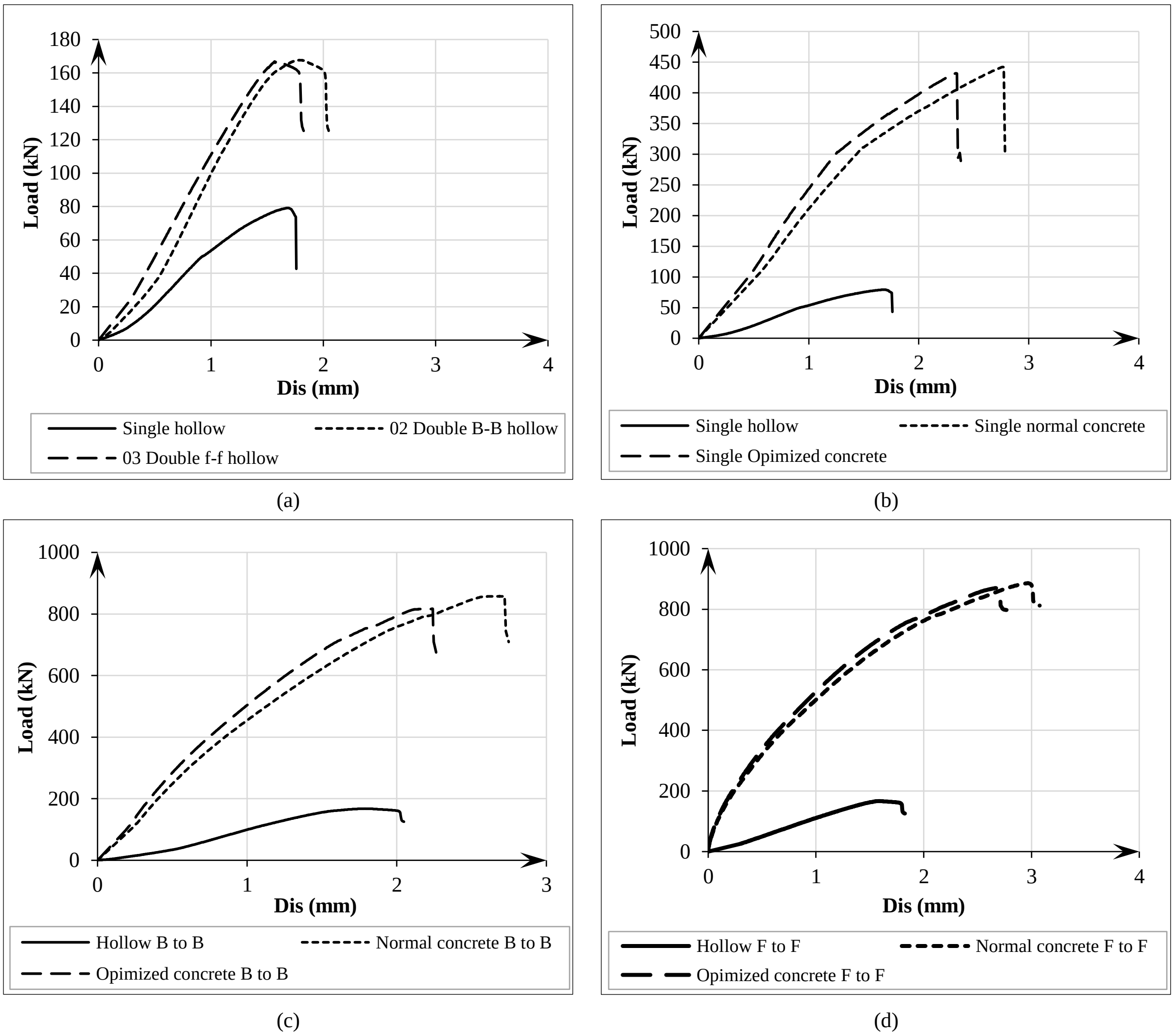

Figure 11. Load x displacement and ultimate load of (a) hollow section (b) SF sections (c) B-B sections (d) F-F sections

Based on these observations, it is evident that the single sections exhibited only half the ultimate load-carrying capacity of the double sections. Among the double-section configurations, the double face-face arrangement demonstrated superior strength and more effective core concrete confinement. The bonded lips in the proposed CFS columns provided seamless integration, functioning effectively as internal stiffeners and delaying the occurrence of top-flange buckling failure.

This mechanism significantly improved the compressive performance of the columns by confining the CFS component, which was protected from buckling deformation by the concrete filling [46]. The double back-to-back C-section exhibited reduced concrete confinement behavior, likely due to the existence of lips at the upper and lower extremities of the pre-engineered cold-formed C-sections, which established a robust connection with the core concrete. These findings indicate that these connectors effectively functioned as internal reinforcements for the upper and lower flanges of the steel tubes in the concrete-filled samples. The performance of the single and double C-section configurations under axial load differs in failure modes. However, considering cost and construction efficiency, the double C-section configuration did not indicate a significant improvement over the single C-section configuration, as the latter provides half the load capacity, which is a reasonable trade-off.

3.4. Load–Strain Relationship

Figure 12 illustrates the connections between the steel C-sections' load and longitudinal strain. When the raw active ingredients were replaced, the load-strain behavior of the specimens filled with recycled material concrete was generally consistent with that of the control specimens. Each specimen had three strain gauges attached to its top, base, and center. Stress (compression load) increased gradually, as indicated by the strain gauge at the top area. A progressive decrease in stress levels was observed at the lower half of the column's cross-section. On the other hand, the strain gauge in the center of the specimen showed a marginal decrease in the related stress. This pattern correlated with the higher motion of the neutral axis in the tested specimens as the compression load increased. The results indicated that the best load-strain performance was observed in the double F-F section, attributed to the full confinement and the role of the lips as internal stiffeners.

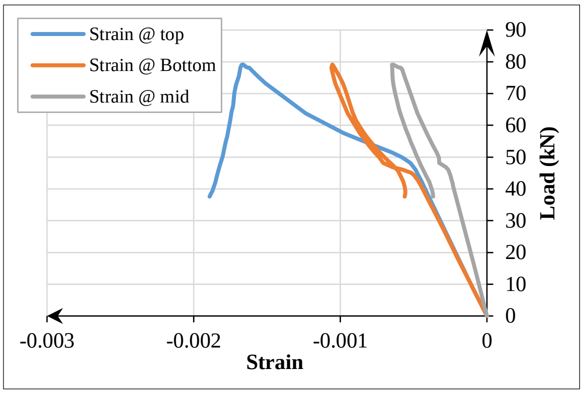

(SH)

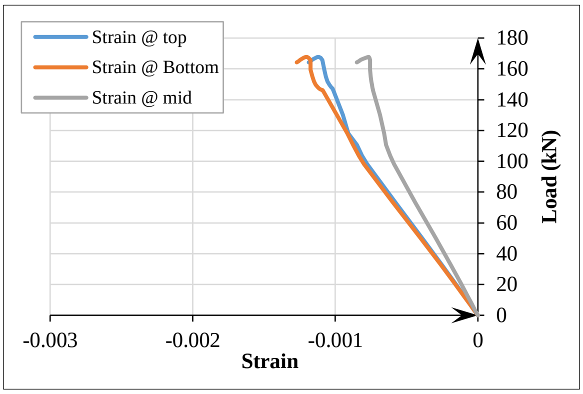

(B-BH)

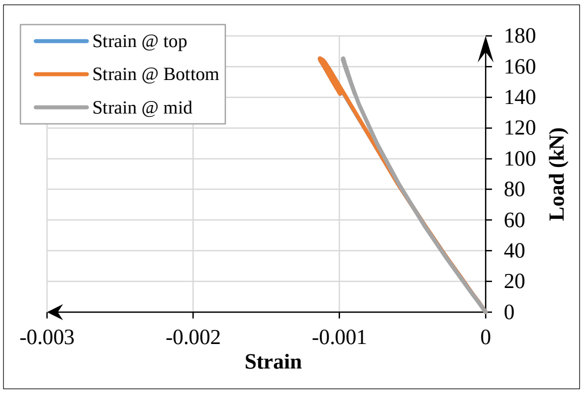

(F-FH)

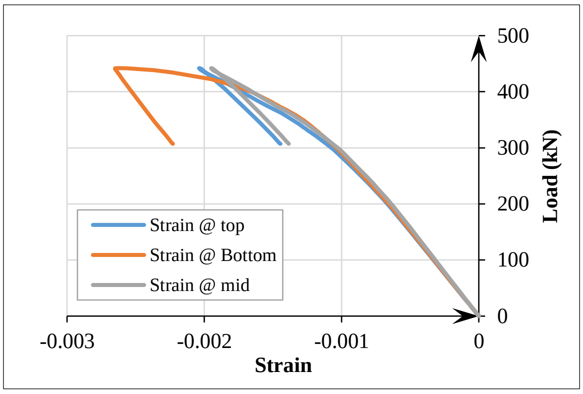

(SFCC)

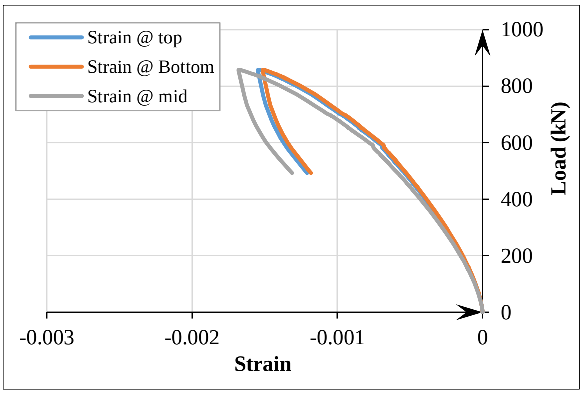

(SFOC)

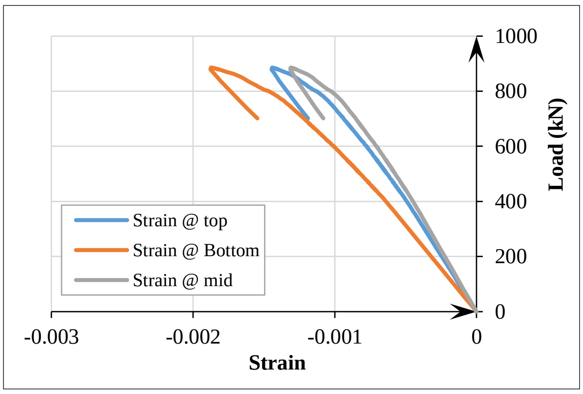

(B-BFCC)

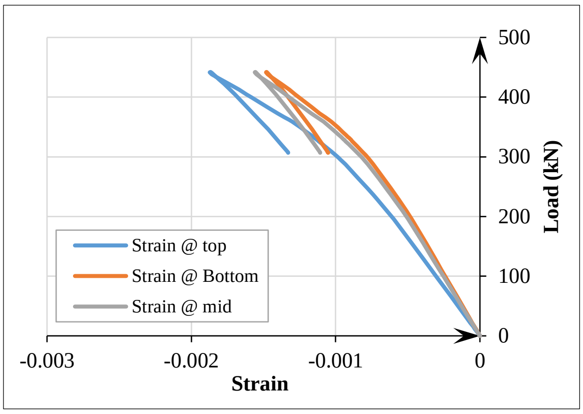

(B-BFOC)

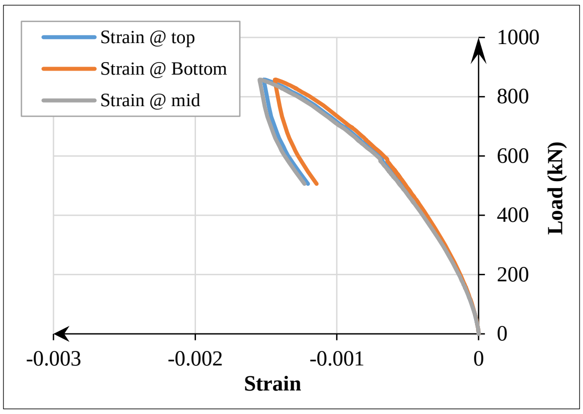

(F-FFCC)

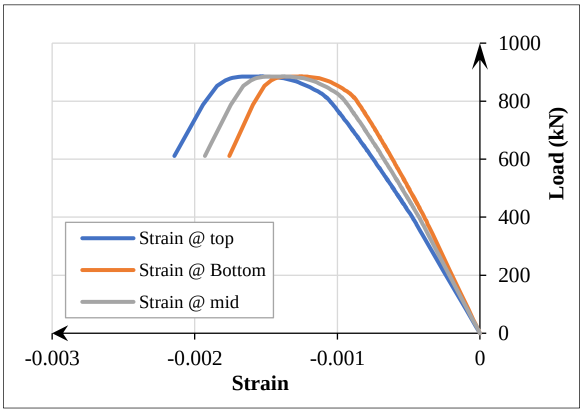

(F-FFOC)

Figure 12. Strain-load relationship of the specimens

3.5. Ductility Index

The ductility index (DI) is based on stresses DI = $\varepsilon_{85\%}/\varepsilon_u$, where $\varepsilon_{85\%}$ is the strain at 85% of the ultimate load and ε_u is the strain at the ultimate load [41]. The ductility of rectangular CFST stub columns improved with an increase in the steel contribution ratio. This section analyzes the DI for the examined specimens, providing essential insights into the overall performance of the newly proposed composite members, as depicted in Figure 13. For compression members, the DI is typically calculated by the ratio of the displacement value at the ultimate limit (Du) to the displacement value at the yielding limit (Dy). The DI results are listed in Table 3. The C-filled section specimens with partially replaced recycled waste material concrete exhibited a slightly higher DI than those filled with control concrete. However, the control concrete-filled specimens demonstrated greater improvement in load capacity compared to those with recycled materials.

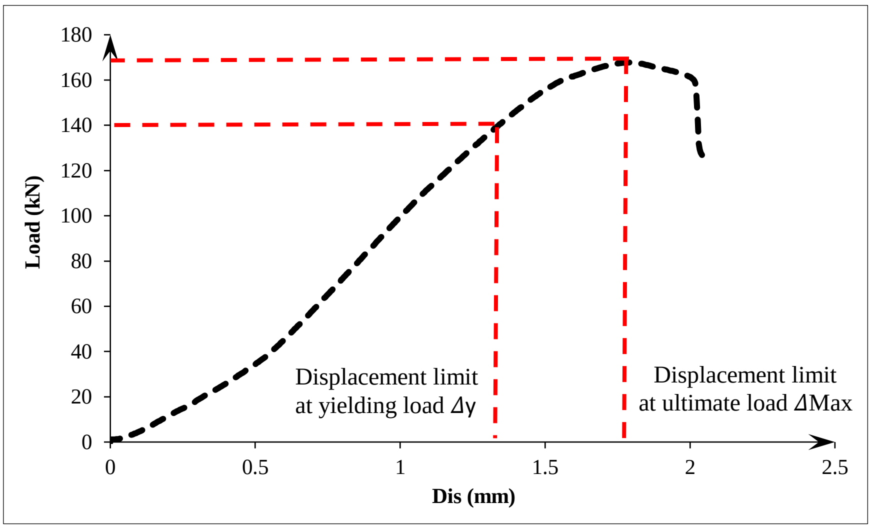

Figure 13. Ductility index DI of double (B-B H) section

Table 3. Ductility index results of the tested specimens

Group No.	Specimens' designation	Ultimate load	Displacement at ultimate load	85% of the ultimate load	Displacement at yielding	DI= $\varepsilon_{85\%}/\varepsilon_u$
Group 1	SH	79.14	1.7	67.2	1.3	0.76
	DB-BH	167.6	1.8	142.46	1.3	0.72
	DF-FH	164.3	1.6	139.6	1.25	0.78
Group 2	SFCC	442.1	2.75	375.7	2	0.72
	DB-BFCC	431.9	2.35	367.1	1.7	0.72
	DF-FFCC	817.6	2.25	694.9	1.53	0.68
Group 3	SFOC	858	2.7	729.3	1.85	0.68
	DB-BFOC	886.4	3	753.4	2	0.66
	DF-FFOC	870.8	2.7	740.1	1.75	0.64

4. Numerical Method

4.1. Description of the Finite Element (FE) Model

The compression behavior of the proposed CFST column was further analyzed using ABAQUS 6.14 software through a non-linear finite element (FE) analysis. The main components of the developed FE CFST models included a concrete infill and steel tube, comprising single and double C-sections. For the concrete component, an eight-node C3D8R element type with six degrees of freedom was employed. The steel tube components were modelled using S4R shell elements. A penalty friction coefficient of 0.5 was selected for the FE analysis to simulate the mechanical interaction between the steel and concrete surfaces. Geometric imperfections in cold-formed C-section steel members can significantly affect their structural performance by reducing load-carrying capacity and stability. Therefore, these imperfections were incorporated into this study better reflect real-world conditions. Addressing these imperfections is essential for ensuring the reliability and safety of structures using these members.

A convergence study was conducted to determine the appropriate friction coefficient. Preliminary FE models with varying friction coefficients (ranging from 0.4 to 0.8), and 0.5 was ultimately established as the optimal value. A similar convergence study was conducted to select the optimal mesh size for the elements in the proposed FE model. The material properties of the steel tube and concrete components in the FE model matched those of the corresponding tested specimens. Concrete, known for its brittleness, was modelled using the "Concrete Damage Plasticity" approach to accurately capture its behavior under tensile and compressive stresses. The elastic properties such as the modulus and Poisson's ratio of the steel component were defined in the elastic-isotropic section, whereas the plastic-isotropic option was used to specify the steel yield strength and corresponding strain values. Constitutive models for the stress-strain relationships of both the steel and concrete materials were applied to ensure the accuracy of the FE CFST models, as shown in Figure 14.

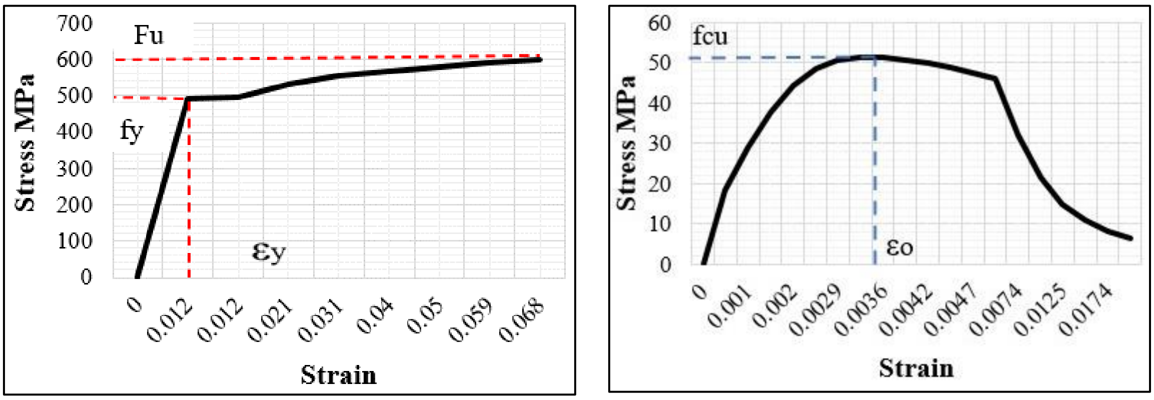

(a) (b)

Figure 14. Stress–strain relation of (a) Steel (b) Concrete

4.2. Validation of the Finite Element (FE) Model

The results of the analyses performed using the developed finite element (FE) model were validated by comparing them with the experimental results of a corresponding specimen (SFNC) using identical material properties. Initially, a convergence study was conducted to determine the optimal element mesh size for the proposed FE model. The purpose of this investigation was to confirm that an increase in the number of elements does not necessarily enhance accuracy.

The numerical analysis showed that the load versus displacement relationship of the SFCC (FE) model agreed sufficiently with that of the tested SFCC specimen, as shown in Figure 15. The axial strength capacity value of the numerical model of SFCC was overestimated by approximately 3.3% (457.2 kN) compared to the value obtained from the tested specimen, as shown in Figure 15-a.

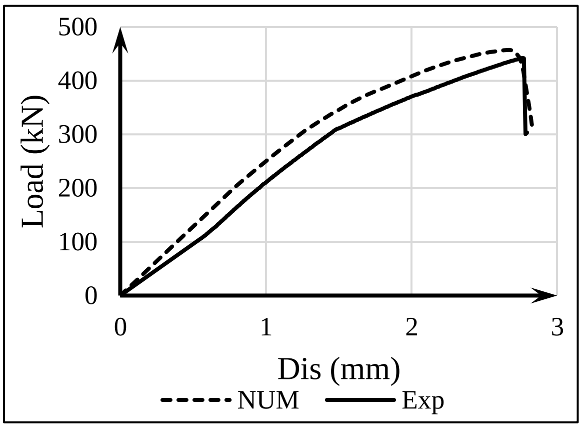

(a)

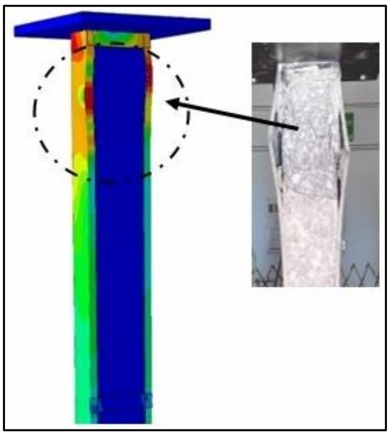

(b)

Figure 15. Results of FE model SFCC: Experiment – numerical (a) load - displacement (b) failure mode

Furthermore, the failure mode and loading capacity identified in the analyzed FE model for all specimens were consistent with the experimental findings, particularly for different column configurations. The failure modes observed in the FE analysis closely matched those seen in the experiments, and the load capacity was also in close agreement. Table 4 lists the experimental and numerical results. Figure 16 compares the failure modes between the experimental and FEA results for hollow C-sections.

Table 4. Summary of the load – displacement of EXP and FE of the specimens

No.	Specimen designation	P EXP	P FE	PEXP / PFE
1.	SH	79.14	82.67	4.36
2.	B-BH	167.7	165.8	1.13
3.	F-FH	164.3	172.3	5.04
4.	SFOC	432.1	450.1	2.28
5.	SFCC	442.04	457.2	3.3
6.	B-BFOC	817.2	847.5	3.6
7.	B-BFN C	858.41	876.1	2.0
8.	F-FFOC	870.3	941.27	7.8
9.	F-FFNC	886.1	917.4	3.4

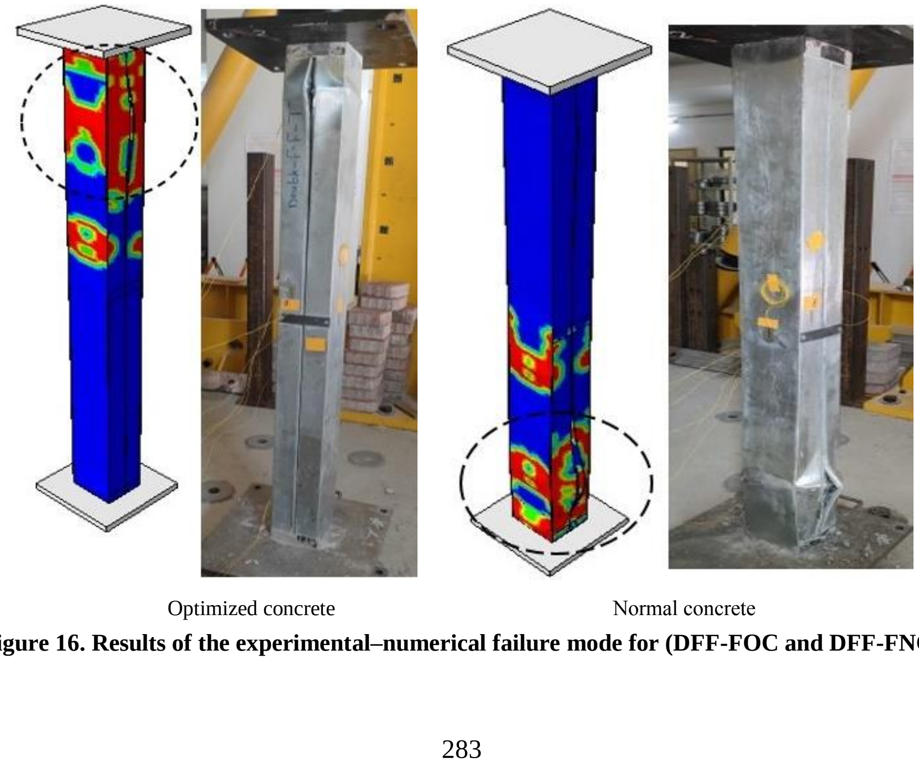

Optimized concrete Normal concrete

Figure 16. Results of the experimental–numerical failure mode for (DFF-FOC and DFF-FNC)

4.3. Parametric Study

This study evaluates several variables, focusing particularly on how steel tube thickness affects the behavior of CFST columns. The relationship between different C-section thicknesses and the compressive performance of recently suggested CFST columns was explored. The study examined several C-sections measuring 1.6, 2.0, 2.5, and 3.0 mm in thickness, which are locally available standards, corresponding to D/t ratios of 100, 75, 60, and 50, respectively. Table 5 presents a summary of the FE results, including displacements at the ultimate load (D) and ultimate load capacity (P).

Table 5. Designation and numerical results of the tube columns thickness

No.	Designation	t (mm)	Length (m)	Depth (mm)	Flange (mm)	Lips (mm)	Load kN
1.	SH	2	1.5	150	65	16	87.4
2.	SH	2.5	1.5	150	65	16	99.3
3.	SH	3	1.5	150	65	16	117.1
4.	B-BH	2	1.5	150	130	16	175.4
5.	B-BH	2.5	1.5	150	130	16	183.1
6.	B-BH	3	1.5	150	130	16	196.7
7.	F-FH	2	1.5	150	130	16	176.2
8.	F-FH	2.5	1.5	150	130	16	191.5
9.	F-FH	3	1.5	150	130	16	199.3
10.	SFCC	2	1.5	150	65	16	487.4
11.	SFCC	2.5	1.5	150	65	16	519.3
12.	SFCC	3	1.5	150	65	16	559.1
13.	SFOC	2	1.5	150	65	16	481.2
14.	SFOC	2.5	1.5	150	65	16	514.3
15.	SFOC	3	1.5	150	65	16	550.5
16.	B-BCC	2	1.5	150	130	16	876.3
17.	B-BCC	2.5	1.5	150	130	16	876.3
18.	B-BCC	3	1.5	150	130	16	876.3
19.	B-BOC	2	1.5	150	130	16	847.7
20.	B-BOC	2.5	1.5	150	130	16	847.7
21.	B-BOC	3	1.5	150	130	16	847.7
22.	F-FCC	2	1.5	150	130	16	917.9
23.	F-FCC	2.5	1.5	150	130	16	931.3
24.	F-FCC	3	1.5	150	130	16	953.7
25.	F-FOC	2	1.5	150	130	16	897.2
26.	F-FOC	2.5	1.5	150	130	16	911.8
27.	F-FOC	3	1.5	150	130	16	924.5

Significant differences were observed in the compressive responses of the concrete-filled C-section models depending on steel thickness. As the thickness of the C-section increased, both stiffness and strength increased significantly, as shown in Figure 17. A FE study showed that a model with a thickness of 1.5 mm for the C-section (D/t = 100) could support an ultimate load of 457.1 kN at a displacement limit of 2.8 mm. In contrast, increasing the thickness to 3 mm (D/t = 50) resulted in a greater load capacity of 559 kN, a 20% increase. This pattern is logical, as outward buckling failure of the C-section gradually decreases with increasing steel thickness, reducing the D/t ratio. The increased thickness enhances concrete confinement, strengthens the steel connections, and allows the lips to act as internal stiffeners along the column, improving both load capacity and buckling resistance. A more optimal thickness of 3 mm may change the shape of the failure modes and delay buckling, owing to the increased cross-sectional area of the steel tubes. Depending on the design, material qualities, and loading conditions, changing the thickness of the column can produce a variety of mechanical and structural results.

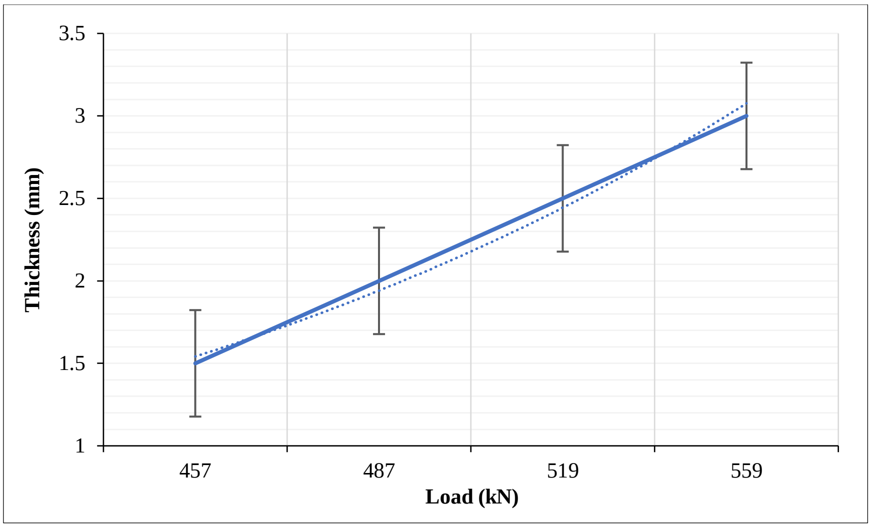

Figure 17. Results of FE models with changing depth-to-thickness ratios

Moreover, the C-section columns with lengths of 1500, 2000, 2500, and 3000 mm, as presented in Table 6, were examined, yielding L/D values of 10, 13.3, 16.6, and 20, respectively. As illustrated in Figure 18, the augmentation of the L/D ratio in the concrete-filled single C-section model resulted in a corresponding decrease in both stiffness and strength. This outcome can be attributed to the inherent relationship between the L/D ratio and the slenderness ratio of the column, where an increase in the L/D ratio signifies higher slenderness of the column. The reduction in cross-sectional area weakens the column, making it more prone to buckling, and thus reducing its load-carrying capacity. Therefore, increasing the length of the column necessitates adjusting the cross-section and steel thickness to maintain stability and prevent buckling.

Table 6. Designation and numerical results of the tube columns length

No.	Designation	t (mm)	Length (m)	Depth (mm)	Flange (mm)	Lips (mm)	Load kN
1.	SH	1.5	2	150	65	16	83.2
2.	SH	1.5	2.5	150	65	16	82.6
3.	SH	1.5	3	150	65	16	82.4
4.	B-BH	1.5	2	150	130	16	172.6
5.	B-BH	1.5	2.5	150	130	16	170.9
6.	B-BH	1.5	3	150	130	16	165.9
7.	F-FH	1.5	2	150	130	16	167.6
8.	F-FH	1.5	2.5	150	130	16	167
9.	F-FH	1.5	3	150	130	16	166.1
10.	SFCC	1.5	2	150	65	16	442.8
11.	SFCC	1.5	2.5	150	65	16	406.7
12.	SFCC	1.5	3	150	65	16	376
13.	SFOC	1.5	2	150	65	16	434.4
14.	SFOC	1.5	2.5	150	65	16	399.8
15.	SFOC	1.5	3	150	65	16	376.4
16.	B-BCC	1.5	2	150	130	16	881.1
17.	B-BCC	1.5	2.5	150	130	16	784.1
18.	B-BCC	1.5	3	150	130	16	741.9
19.	B-BOC	1.5	2	150	130	16	852.4
20.	B-BOC	1.5	2.5	150	130	16	808.1
21.	B-BOC	1.5	3	150	130	16	771.1
22.	F-FCC	1.5	2	150	130	16	909.4
23.	F-FCC	1.5	2.5	150	130	16	870.2
24.	F-FCC	1.5	3	150	130	16	722.06
25.	F-FOC	1.5	2	150	130	16	903.1
26.	F-FOC	1.5	2.5	150	130	16	861.2
27.	F-FOC	1.5	3	150	130	16	745.2

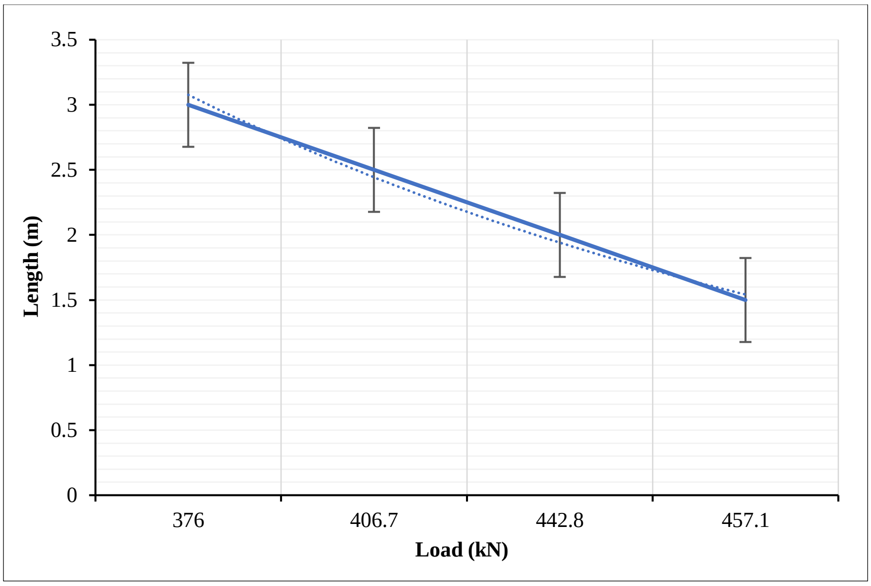

Figure 18. Results of FE models with changing length ratios

For example, the control model with an L/D ratio of 10 (L = 1500 mm) had a load capacity of 457.1 kN. As the L/D increased, the loading capacity decreased at higher displacement, with an L/D ratio of 13.3 (L = 2000 mm) achieving 442.8 kN, an L/D ratio of 16.6 (L = 2500 mm) reaching 406.7 kN, and an L/D ratio of 20 (L = 3000 mm) achieving 376 kN. As the length of a column increases, both capacity and susceptibility to buckling are affected. The response of a CFST column to changes in length must consider structural stability, buckling, and load-carrying capacity.

5. Conclusions

This study evaluated the compression performance of CFST columns constructed from single and double C-sections. These sections were either hollow or filled with various recycled concrete mixtures in addition to regular concrete mixes. The findings of this analysis are summarized as follows:

- Recycled waste materials can produce high-performance concrete with specified contents (10% WGP, 8% HDPE beads, and 10% PSA). These percentages were used to create an optimized mix that replaced portions of the concrete material.
- The axial load capacity of a single C-section CFS filled with concrete increased by more than five times compared to the hollow section when using a concrete mixture containing 28% recycled materials (10% WGP, 8% HDPE beads, and 10% PSA). This improvement is attributed to the effect of the infill concrete material, which prevented early buckling failure.
- The double face-to-face arrangement demonstrated superior strength and enhanced core concrete confinement. The bonded lips in the proposed CFST columns resulted in seamless integration, which functioned effectively as internal stiffeners, delaying the occurrence of top-flange buckling failure and significantly improving the compressive performance of the columns.
- In contrast, the double B-B section columns exhibited reduced load-carrying capacity compared to the double face-to-face section. This decrease is attributed to the open nature of the section on both sides, which failed to completely confine the concrete.
- While the single and double C-section configurations did not differ significantly in terms of load capacity, the single C-column had approximately half of the double C-section. However, in terms of buckling, the double C-section predicted a greater delay compared to the single section.
- Steel strips used to connect the lips of the C-section flanges enhanced the axial strength of the single-filled column by approximately 2% compared to the unstrengthened specimen. The steel strips also delayed buckling at vulnerable locations. Increasing the number of steel strips in the loading and support areas further enhanced resistance to buckling and load capacity.
- The failure modes of the specimens filled with the control concrete occurred at the bottom (support), whereas those filled with the optimized concrete failed at the top (loading area). Both mixtures showed similar performance. The failure modes in the single C-section in a concrete-filled tube composite system differed from those in two C-purlins joined together, due to challenges in confining the infill concrete.

- The ultimate load capacity and failure mode of a single C-section filled with concrete with a thickness of 1.5 mm (D/t = 100), achieving 457.1 kN, were verified using FE analysis. The FE study findings showed that the load capacity and behavior of the concrete-filled C-sections were significantly improved with a small reduction in the D/t ratio. Additionally, a 20% improvement in load capacity was observed when the thickness was increased to 3 mm (D/t = 50). Increasing the L/D ratio reduced loading capacity. Buckling can be affected, and the response of a CFST column to changes in length involves considerations related to structural stability, buckling, and load-carrying capacity. Buckling is a stable failure that exhibits high susceptibility to buckling.

Finally, further experimental and numerical evaluations are required to investigate additional parameters that remain unexplored. These parameters encompass variations in the size and length of the C-section, increasing the implementation of steel strips and refining connection methodologies to better understand the compression performance of the proposed tubular steel columns (single and double C-purlins).

6. Abbreviation

fcu (MPa)	Concrete cube compressive strength	S	Single
fck (MPa)	Characteristic concrete strength (0.67fcu)	D	Double
Le (mm)	Effective length of specimen	H	Hollow
t (mm)	Thickness of steel tube	F	Filled
L (mm)	Lip	SH	Single Hollow
d (mm)	Web	SF	Single Filled
b (mm)	Flange	CFST	Concrete-Filled Steel Tube
DI	Ductility Index	CFS	Cold Formed Steel
Fu (MPa)	Ultimate strength of steel	SFCC	Single Filled Control Concrete
fy (MPa)	Yield strength of steel	SFOC	Single Filled Optimized Concrete
E (GPa)	Modulus of elasticity for concrete	DB-BH	Double Back-to-Back Hollow
ε	Strain at relevant concrete compression stress	B-BFCC	Back-to-Back Filled Control Concrete
W	C-section width	B-BFOC	Back-to-Back Filled Optimized Concrete
D/t	Depth / thickness ratio	DF-FH	Double Face-to-Face Hollow
L/D	Length / depth ratio	F-FFCC	Face -to-Face Filled Control Concrete
P (kN)	Ultimate load	F-FFOC	Face-to-Face Filled Optimized Concrete
dis (mm)	Displacement mm	CC	Control Concrete
WGP	Waste Glass Powder	OC	Optimized Concrete
HDPE	High Density Polyethylene	FCC	Filled Control Concrete
PSA	Pumice Stone Aggregate	FOC	Filled Optimized Concrete

7. Declarations

7.1. Author Contributions

Conceptualization, A.D.A.J.; methodology, L.S.W.; software, A.D.A.J.; validation, L.S.W., A.W.A., and S.Y.K.; formal analysis, A.D.A.J.; investigation, A.D.A.J. and S.Y.K.; resources, A.D.A.J.; data curation, A.W.A. and S.Y.K.; writing—original draft preparation, A.D.A.J.; writing—review and editing, A.W.A. and S.Y.K.; visualization, A.W.A. and S.Y.K.; supervision, L.S.W.; project administration, A.D.A.J.; funding acquisition, L.S.W. All authors have read and agreed to the published version of the manuscript.

7.2. Data Availability Statement

Data sharing is not applicable to this article.

7.3. Funding

The authors gratefully acknowledge the financial support for this research, provided through the Fundamental Research Grant Scheme (FRGS) under grant number FRGS/1/2022/TK01/UNITEN/02/1, funded by the Malaysian Ministry of Higher Education.

7.4. Conflicts of Interest

The authors declare no conflict of interest.

8. References

[1] Zong, Z. H., Jaishi, B., Ge, J. P., & Ren, W. X. (2005). Dynamic analysis of a half-through concrete-filled steel tubular arch bridge. Engineering Structures, 27(1), 3–15. doi:10.1016/j.engstruct.2004.08.007.

[2] Han, L. H., Li, W., & Bjorhovde, R. (2014). Developments and advanced applications of concrete-filled steel tubular (CFST) structures: Members. Journal of Constructional Steel Research, 100, 211–228. doi:10.1016/j.jcsr.2014.04.016.

[3] Wu, D., Gao, W., Feng, J., & Luo, K. (2016). Structural behaviour evolution of composite steel-concrete curved structure with uncertain creep and shrinkage effects. Composites Part B: Engineering, 86, 261–272. doi:10.1016/j.compositesb.2015.10.004.

[4] Gao, J., Su, J., Xia, Y., & Chen, B. (2014). Experimental study of concrete-filled steel tubular arches with corrugated steel webs. Advanced Steel Construction, 10(1), 99–115. doi:10.18057/ijasc.2014.10.1.7.

[5] Elchalakani, M., Zhao, X. L., & Grzebieta, R. H. (2001). Concrete-filled circular steel tubes subjected to pure bending. Journal of Constructional Steel Research, 57(11), 1141–1168. doi:10.1016/S0143-974X(01)00035-9.

[6] Ren, Q. X., Han, L. H., Lam, D., & Li, W. (2014). Tests on elliptical concrete filled steel tubular (CFST) beams and columns. Journal of Constructional Steel Research, 99, 149–160. doi:10.1016/j.jcsr.2014.03.010.

[7] Wang, R., Han, L. H., Nie, J. G., & Zhao, X. L. (2014). Flexural performance of rectangular CFST members. Thin-Walled Structures, 79, 154–165. doi:10.1016/j.tws.2014.02.015.

[8] Zhang, Y. B., Han, L. H., Zhou, K., & Yang, S. (2019). Mechanical performance of hexagonal multi-cell concrete-filled steel tubular (CFST) stub columns under axial compression. Thin-Walled Structures, 134, 71–83. doi:10.1016/j.tws.2018.09.027.

[9] Javed, M. F., Sulong, N. H. R., Memon, S. A., Rehman, S. K. U., & Khan, N. B. (2017). FE modelling of the flexural behaviour of square and rectangular steel tubes filled with normal and high strength concrete. Thin-Walled Structures, 119, 470–481. doi:10.1016/j.tws.2017.06.025.

[10] Su, S., Li, X., Wang, T., & Zhu, Y. (2016). A comparative study of environmental performance between CFST and RC columns under combinations of compression and bending. Journal of Cleaner Production, 137, 10–20. doi:10.1016/j.jclepro.2016.07.043.

[11] Saadeh, M., & Irshidat, M. R. (2024). Recent advances in concrete-filled fiber-reinforced polymer tubes: a systematic review and future directions. Innovative Infrastructure Solutions, 9(11), 406. doi:10.1007/s41062-024-01722-z.

[12] Senthilkumar, R., Karunakaran, P., & Chandru, U. (2023). Progress and challenges in double skin steel–concrete composite walls: a review. Innovative Infrastructure Solutions, 8(1), 32. doi:10.1007/s41062-022-00973-y.

[13] Shen, Y., & Tu, Y. (2021). Flexural strength evaluation of multi-cell composite T-shaped concrete-filled steel tubular beams. Materials, 14(11), 2838. doi:10.3390/ma14112838.

[14] Shen, Y., Tu, Y., & Huang, W. (2022). Flexural Strength Evaluation of Multi-Cell Composite L-Shaped Concrete-Filled Steel Tubular Beams. Buildings, 12(1), 39. doi:10.3390/buildings12010039.

[15] Jasim Hilo, S., Wan Badaruzzaman, W. H., Osman, S. A., & Al Zand, A. W. (2015). Axial Load Behavior of Acomposite Wall Strengthened with an Embedded Octagon Cold-Formed Steel. Applied Mechanics and Materials, 754–755, 437–441. doi:10.4028/www.scientific.net/amm.754-755.437.

[16] Al-Shaikhli, M. S., Badaruzzaman, W. H. W., & Al Zand, A. W. (2022). Experimental and numerical study on the PSSDB system as two-way floor units. Steel and Composite Structures, 42(1), 33–48. doi:10.12989/scs.2022.42.1.033.

[17] Dai, Y., Roy, K., Fang, Z., Chen, B., Raftery, G. M., & Lim, J. B. P. (2024). Buckling resistance of axially loaded cold-formed steel built-up stiffened box sections through experimental testing and finite element analysis. Engineering Structures, 302, 117379. doi:10.1016/j.engstruct.2023.117379.

[18] He, Z., Peng, S., Zhou, X., Li, Z., Yang, G., & Zhang, Z. (2024). Design recommendation of cold-formed steel built-up sections under concentric and eccentric compression. Journal of Constructional Steel Research, 212, 108255. doi:10.1016/j.jcsr.2023.108255.

[19] Yang, J., Luo, K., Wang, W., Shi, Y., & Li, H. (2024). Axial compressive behavior of cold-formed steel built-up box-shape columns with longitudinal stiffeners. Journal of Constructional Steel Research, 212, 108274. doi:10.1016/j.jcsr.2023.108274.

[20] Yılmaz, Y., Öztürk, F., & Demir, S. (2024). Buckling behavior of cold-formed steel sigma and lipped channel section beam-columns: Experimental and numerical investigation. Journal of Constructional Steel Research, 214, 108456. doi:10.1016/j.jcsr.2024.108456.

[21] Kumar, N., & Sahoo, D. R. (2016). Optimization of lip length and aspect ratio of thin channel sections under minor axes bending. Thin-Walled Structures, 100, 158–169. doi:10.1016/j.tws.2015.12.015.

[22] Adil Dar, M., Subramanian, N., Anbarasu, M., Dar, A. R., & Lim, J. B. P. (2018). Structural performance of cold-formed steel composite beams. Steel and Composite Structures, 27(5), 545–554. doi:10.12989/scs.2018.27.5.545.

[23] Al Zand, A. W., Alghaaeb, M. F., Liejy, M. C., Mutalib, A. A., & Al-Ameri, R. (2022). Stiffening Performance of Cold-Formed C-Section Beam Filled with Lightweight-Recycled Concrete Mixture. Materials, 15(9), 2982. doi:10.3390/ma15092982.

[24] Al Zand, A. W., Badaruzzaman, W. H. W., Mutalib, A. A., & Hilo, S. J. (2018). Flexural Behavior of CFST Beams Partially Strengthened with Unidirectional CFRP Sheets: Experimental and Theoretical Study. Journal of Composites for Construction, 22(4), 4018018. doi:10.1061/(asce)cc.1943-5614.0000852.

[25] Al Zand, A. W., Ali, M. M., Al-Ameri, R., Badaruzzaman, W. H. W., Tawfeeq, W. M., Hosseinpour, E., & Yaseen, Z. M. (2021). Flexural strength of internally stiffened tubular steel beam filled with recycled concrete materials. Materials, 14(21), 6334. doi:10.3390/ma14216334.

[26] Ahmed, W., & Lim, C. W. (2021). Production of sustainable and structural fiber reinforced recycled aggregate concrete with improved fracture properties: A review. Journal of Cleaner Production, 279, 279. doi:10.1016/j.jclepro.2020.123832.

[27] Liu, Z., Lu, Y., Li, S., Zong, S., & Yi, S. (2020). Flexural behavior of steel fiber reinforced self-stressing recycled aggregate concrete-filled steel tube. Journal of Cleaner Production, 274, 274. doi:10.1016/j.jclepro.2020.122724.

[28] Fahmy, M. F. M., & Idriss, L. K. (2019). Flexural behavior of large scale semi-precast reinforced concrete T-beams made of natural and recycled aggregate concrete. Engineering Structures, 198. doi:10.1016/j.engstruct.2019.109525.

[29] Zhang, H., Geng, Y., Wang, Y. Y., & Wang, Q. (2020). Long-term behavior of continuous composite slabs made with 100% fine and coarse recycled aggregate. Engineering Structures, 212, 212. doi:10.1016/j.engstruct.2020.110464.

[30] Yang, Y. F., & Han, L. H. (2006). Experimental behaviour of recycled aggregate concrete filled steel tubular columns. Journal of Constructional Steel Research, 62(12), 1310–1324. doi:10.1016/j.jcsr.2006.02.010.

[31] Yang, Y. F., & Man, L. H. (2006). Compressive and flexural behaviour of recycled aggregate concrete filled steel tubes (RACFST) under short-term loadings. Steel and Composite Structures, 6(3), 257–284. doi:10.12989/scs.2006.6.3.257.

[32] Yang, Y. F., & Zhu, L. T. (2009). Recycled aggregate concrete filled steel SHS beam-columns subjected to cyclic loading. Steel and Composite Structures, 9(1), 19–38. doi:10.12989/scs.2009.9.1.019.

[33] Hamada, H., Alattar, A., Tayeh, B., Yahaya, F., & Thomas, B. (2022). Effect of recycled waste glass on the properties of high-performance concrete: A critical review. Case Studies in Construction Materials, 17, 1149. doi:10.1016/j.cscm.2022.e01149.

[34] Ahmed, K. S., & Rana, L. R. (2023). Fresh and hardened properties of concrete containing recycled waste glass: A review. Journal of Building Engineering, 70, 1063127. doi:10.1016/j.jobe.2023.106327.

[35] Balasubramanian, B., Gopala Krishna, G. V. T., Saraswathy, V., & Srinivasan, K. (2021). Experimental investigation on concrete partially replaced with waste glass powder and waste E-plastic. Construction and Building Materials, 278, 278. doi:10.1016/j.conbuildmat.2021.122400.

[36] Abeysinghe, S., Gunasekara, C., Bandara, C., Nguyen, K., Dissanayake, R., & Mendis, P. (2021). Engineering performance of concrete incorporated with recycled high-density polyethylene (HDPE)—A systematic review. Polymers, 13(11), 1885. doi:10.3390/polym13111885.

[37] Tamrin, & Nurdiana, J. (2021). The effect of recycled HDPE plastic additions on concrete performance. Recycling, 6(1), 1–19. doi:10.3390/recycling6010018.

[38] Karthika, R. B., Vidyapriya, V., Nandhini Sri, K. V., Merlin Grace Beaula, K., Harini, R., & Sriram, M. (2020). Experimental study on lightweight concrete using pumice aggregate. Materials Today: Proceedings, 43, 1606–1613. doi:10.1016/j.matpr.2020.09.762.

[39] Kurt, M., Kotan, T., GüL, M. S., GüL, R., & Aydin, A. C. (2016). The effect of blast furnace slag on the self-compactability of pumice aggregate lightweight concrete. Sadhana - Academy Proceedings in Engineering Sciences, 41(2), 253–264. doi:10.1007/s12046-016-0462-2.

[40] Metwally, I. M. (2007). Investigations on the performance of concrete made with blended finely milled waste glass. Advances in Structural Engineering, 10(1), 47–53. doi:10.1260/136943307780150823.

[41] Yu, C. Q., Tong, J. Z., & Tong, G. S. (2021). Behavior and design of slender concrete-filled wide rectangular steel tubular columns under axial compression. Structures, 33, 3137–3146. doi:10.1016/j.istruc.2021.06.065.

[42] Ravi Kumar B. S., Chandan M. B., Dayananda, N. S., Sunil Kumar, M. M., & Akarsh H. R. (2017). An Experimental Study on Lightweight Concrete by Partially Replacing of Normal Coarse Aggregate by Pumice Stone. International Journal for Scientific Research and Development, 5(2), 1982–1985.

[43] Zhu, A., Zhang, X., Zhu, H., Zhu, J., & Lu, Y. (2017). Experimental study of concrete filled cold-formed steel tubular stub columns. Journal of Constructional Steel Research, 134, 17–27. doi:10.1016/j.jcsr.2017.03.003.

[44] Al Zand, A. W., Wan Badaruzzaman, W. H., Ali, M. M., Hasan, Q. A., & Al-Shaikhli, M. S. (2020). Flexural performance of cold-formed square CFST beams strengthened with internal stiffeners. Steel and Composite Structures, 34(1), 123–139. doi:10.12989/scs.2020.34.1.123.

[45] Lu, Y., Zhou, T., Li, W., & Wu, H. (2017). Experimental investigation and a novel direct strength method for cold-formed built-up I-section columns. Thin-Walled Structures, 112, 125–139. doi:10.1016/j.tws.2016.12.011.

[46] Rahnavard, R., Craveiro, H. D., Lopes, M., Simões, R. A., Laím, L., & Rebelo, C. (2022). Concrete-filled cold-formed steel (CF-CFS) built-up columns under compression: Test and design. Thin-Walled Structures, 179, 109603. doi:10.1016/j.tws.2022.109603.